Local unified models of backscattering from ocean-like surfaces at moderate incidence angles

Nicolas Pinel, Christophe Bourlier

LOCAL UNIFIED MODELS OF BACKSCATTERING FROM OCEAN-LIKE SURFACES AT MODERATE INCIDENCE ANGLES

Nicolas Pinel and Christophe Bourlier
IREENA Laboratory – Radar Team
Polytech'Nantes, Université de Nantes
Nantes, France
nicolas.pinel@gmail.com, christophe.bourlier@univ-nantes.fr

***Abstract*— In the context of electromagnetic wave backscattering from ocean-like surfaces, by using the SSA-1 model, Bourlier et al. proposed a technique to reduce the number of numerical integrations to two for easier numerical implementation. To be consistent with microwave measurements, closed-form expressions of the Fourier coefficients of the backscattering RCS are obtained. For Gaussian statistics, previous work is extended to kernels of unified models expanded up to the order two, like the SSA2 and LCA2.**

Electromagnetic scattering by rough surfaces, Random media, Sea surface, Water pollution, Multistatic scattering

I. INTRODUCTION

From the 1960s, the derivation of the microwave backscattering normalized radar cross section (BNRCS) from ocean surfaces is a topic of investigation which makes progress and remains a challenging task. The first developed model is the TSM [1, 2]. Recently, this approach was improved [3–5]. In the last two decades, another group of scattering models was proposed, namely the *local unified* models. The term *local* means that the multiple scattering phenomenon is neglected, and the term *unified* means that the model satisfies the high- and low- frequency limits, given by the geometric optics approximation (GOA) and the small perturbation method (SPM), respectively. For more details, see the thorough review of Elfouhaily and Guérin [6]. One of the most popular is the SSA2 published by Voronovich [7, 8, 9]; more recently, models based on the same decomposition of the scattering matrix as SSA2, like the LCA2, were published by Elfouhaily et al. [10, 11].

It is well known that such backscattering models are extremely difficult to implement in the full three-dimensional case, because of the four-fold integral that is involved (two space variables and two frequency variables) and because of the strongly oscillating behavior of the integrand. That is why, recently, Bourlier and Pinel presented [12, 13] an original technique to reduce this computation to a two-fold integral (one space variable and one frequency variable) by resorting to azimuthal harmonic expansion of the BNRCS and by using Bessel functions. This is done for two-harmonic spectra such as the Elfouhaily et al. spectrum [14].

In this paper, this model is presented and tested for microwave frequencies and different wind speeds. The paper is organized as follows. In section 2, the technique developed by Bourlier and Pinel is briefly summarized, and in section 3, the BNRCS is compared with its first order, easier to compute than the second order. The last section gives concluding remarks.

II. BNRCS OF UNIFIED SCATTERING MODELS

In the literature, from microwave (C and K_u bands for instance) experimental data [15, 16, 17], it was established that the BNRCS σ^{pq} can be expressed for pq={VV,HH} co-polarizations in the form

$$\sigma^{pq}(\theta,\phi;u)=\sigma_0^{pq}(\theta;u)+\sigma_1^{pq}(\theta;u)\cos\phi+\sigma_2^{pq}(\theta;u)\cos(2\phi)$$

where ϕ is the observation azimuthal angle with respect to the wind direction, θ the observation elevation angle, and u the wind speed. The isotropic backscattering term σ_0^{pq} mainly describes the wind speed, σ_1^{pq} the surface asymmetry between the up (ϕ=0) and down (ϕ=180°) wind directions, and σ_2^{pq} the surface asymmetry between the up (ϕ=0) and cross (ϕ=90°) wind directions. For Gaussian statistics, σ_1^{pq}=0. Non-Gaussian statistics is addressed in [12] by considering only the SSA-1 kernel.

By considering the first two orders of the kernels of unified models, $\hat{\mathcal{N}}^{pq}(-\mathbf{k}_0,\mathbf{k}_0;\boldsymbol{\xi})\approx\mathcal{N}_1^{pq}(-\mathbf{k}_0,\mathbf{k}_0)+\hat{\mathcal{N}}_2^{pq}(-\mathbf{k}_0,\mathbf{k}_0;\boldsymbol{\xi})$, which depend on the chosen model, the NRBCS is then equal to the sum of two terms, $\sigma^{pq}=\sigma_{11}^{pq}+\sigma_{12}^{pq}$. The subscript "11" results from the correlation of the first-order scattered field, whereas the subscript "12" results from the cross-correlation between the first- and second- order scattered fields. The vectors $\mathbf{k}_0$ and $\mathbf{k}$ (boldface denotes a vector) are the horizontal components of the incident and the scattered waves (whereas q_0 and q_k are the vertical ones, see figure 1).

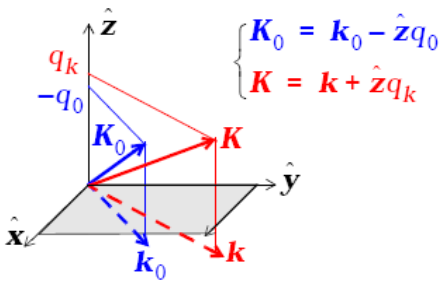

Figure 1. Geometry of the problem

By assuming Gaussian statistics, Bourlier and Pinel [13] recently showed that the BNRCS harmonics $\{\sigma^{pq}_{11,0}(\theta;u), \sigma^{pq}_{11,1}(\theta;u), \sigma^{pq}_{11,2}(\theta;u)\}$ related to "11" can be expressed as

$$\begin{cases} \sigma^{pq}_{11,0}(\theta;u) = 2\pi A \left|\mathcal{N}^{pq}_1(\theta)\right|^2 e^{-Q_z^2\sigma_\eta^2} \int_0^\infty J_0(k_B r)\left[e^{Q_z^2 W_0(r)} I_0\left(Q_z^2 W_2(r)\right) - 1\right] r dr \\ \sigma^{pq}_{11,1}(\theta;u) = 0 \\ \sigma^{pq}_{11,2}(\theta;u) = 4\pi A \left|\mathcal{N}^{pq}_1(\theta)\right|^2 e^{-Q_z^2\sigma_\eta^2} \int_0^\infty e^{Q_z^2 W_0(r)} J_2(k_B r) I_1\left(Q_z^2 W_2(r)\right) r dr \end{cases}$$

where

$$\begin{cases} W_2(r,\phi_r) = W_0(r) - \cos(2\phi_r) W_2(r) \\ W_0(r) = \int_0^\infty \hat{W}_0(\xi) J_0(r\xi) d\xi \\ W_2(r) = \int_0^\infty \hat{W}_2(\xi) J_2(r\xi) d\xi \end{cases}$$

and $A=1/(\pi Q_z^2)$, $Q_z = 2K\cos\theta$, $k_B = 2K\sin\theta$, $K=2\pi/\lambda$, in which λ is the radar wavelength. $W_0(r)$ and $W_2(r)$ stand for the isotropic and anisotropic parts of the height autocorrelation function, respectively. The hat over W, as a function of ξ, corresponds to the associated spectrum. In polar coordinates (ξ,ϕ_ξ), the sea spectrum is assumed to be $\hat{W}(\xi,\phi_\xi) = [\hat{W}_0(\xi) + \hat{W}_0(\xi)\cos(2\phi_\xi)]/(2\pi)$, which is consistent with the Elfouhaily et al. sea spectrum [14]. J_m and I_m are the Bessel functions of the first and second kinds, respectively, and of order m. The above equations show that the BNRCS is obtained from a single numerical integration over the radial distance r, instead of two, with one over r and one over an angular variable. Thus, the numerical evaluation of the order "11" is rather simple. For the SSA model, N_1^{pq} is given by the SPM model, whereas for the LCA model, it is given by the Kirchhoff approximation model. Their expression can be found in [13].

For the LCA2 model, we have (ν=0)

$$\begin{aligned} \sigma^{pq}_{12,n}(\theta;u) &= 2A\pi e^{-Q_z^2\sigma_\eta^2} \int_0^\infty \int_0^\infty r d\xi dr \hat{G}^{pq}_0(\xi) \\ &\times \left(\hat{W}_0(\xi) J_n(a) \left\{ e^{Q_z^2 W_0(r)} I_{\frac{n}{2}}(b) \left[J_0(c) - 1\right] + \delta_{n,0} \right\} \right. \\ &\left. + \frac{1}{2} \hat{W}_2(\xi) e^{Q_z^2 W_0(r)} J_n(a) J_2(c) \left[I_{\frac{n-2}{2}}(b) + I_{\frac{n+2}{2}}(b) \right] \right), n \text{ even} \end{aligned} \quad (1)$$

where

$$\hat{G}^{pq}_s(\xi) = \frac{1}{2\pi} \int_0^{2\pi} \hat{G}^{pq}(\xi, \phi_\xi - \nu\phi) e^{-js(\phi_\xi - \nu\phi)} d(\phi_\xi - \nu\phi) \quad (2)$$

$$\begin{cases} \hat{G}^{pq}(\xi,\phi_\xi) = -2Q_z \mathrm{Im}\left[(\mathcal{N}^{pq}_1)^* \hat{\mathcal{N}}^{pq}_2(\xi,\phi_\xi) \right] \\ \hat{G}^{pq}(\xi,\phi_\xi) = -2Q_z \mathrm{Im}\left[(\mathcal{N}^{pq}_1)^* \hat{\mathcal{N}}^{pq}_2(\xi,\phi_\xi) \right] + \left| \hat{\mathcal{N}}^{pq}_2(\xi,\phi_\xi) \right|^2 \quad \text{PPT} \end{cases} \quad (3)$$

$$a = k_B r = 2Kr\sin\theta,\ b = Q_z^2 W_2(r),\ c = \xi r$$

and $\delta_{n,m}$ is the Kronnecker Symbol, such that $\delta_{n,m}=1$ if n=m ; 0 otherwise.

Equation (2) is the Fourier series of the kernel $\hat{G}^{pq}(\xi,\phi_\xi)$ expressed from the first- $\mathcal{N}^{pq}_1(-\mathbf{k}_0,\mathbf{k}_0)$ and second- $\mathcal{N}^{pq}_2(-\mathbf{k}_0,\mathbf{k}_0;\xi,\phi_\xi)$ order kernels. In the backscattering direction, their expression can be found in [13]. To simplify the derivation of the BNRCS, the PPT is often applied, which implies a new definition of the kernel $\hat{G}^{pq}(\xi,\phi_\xi)$. Under the PPT, in Eq. (3), the term $\hat{G}^{pq}(\xi,\phi_\xi)$ is derived from the BNRCS (for instance, see Eqs. (21) and (22) of [13]) by using the series expansion $e^x \approx 1+x$. By comparison, the scattered field (for instance, see Eq. (10) of [13]) derived under the PPT uses the reverse way, that is to say the approximation $1+x \approx e^x$.

For the SSA2 model, we have (ν=1)

$$\begin{aligned} \sigma^{pq}_{12,n}(\theta;u) &= 2A\pi e^{-Q_z^2\sigma_\eta^2} \int_0^\infty \int_0^\infty r d\xi dr \\ &\times \left(\hat{W}_0(\xi) \left\{ e^{Q_z^2 W_0(r)} \left[\Omega^{(0)}_n(a,b,c) - \hat{G}^{pq}_0(\xi) I_{\frac{n}{2}}(b) J_n(a) \right] + \hat{G}^{pq}_0(\xi) J_0(a) \delta_{n,0} \right\} \right. \\ &+ \hat{W}_2(\xi) \left\{ e^{Q_z^2 W_0(r)} \left[\Omega^{(2)}_n(a,b,c) - \hat{G}^{pq}_2(\xi) \sum_{\gamma=\pm1} J_{n\gamma+2}(a) I_{\frac{n\gamma+2}{2}}(b) \right] \right. \\ &\left. \left. + \hat{G}^{pq}_2(\xi) J_0(a) \delta_{n,\pm2} \right\} \right), n \text{ even}, \end{aligned} \quad (4)$$

where

$$\Omega_n^{(0)}(a,b,c) = \sum_{s=-\infty}^{+\infty} \frac{(-1)^s \hat{G}_s^{pq}(\xi)}{2} J_s(c) \left[\sum_{\gamma=\pm 1} J_{n\gamma+s}(a) I_{\frac{n\gamma}{2}}(b) \right] =$$

$$\hat{G}_0^{pq}(\xi) J_0(c) J_n(a) I_{\frac{n}{2}}(b)$$

$$+ \sum_{s=1}^{+\infty} \hat{G}_s^{pq}(\xi) J_s(c) I_{\frac{n}{2}}(b) \left[(-1)^s J_{n+s}(a) + J_{n-s}(a) \right] n \text{ even; } 0 \text{ otherwise}$$

and

$$\Omega_n^{(2)}(a,b,c) = \sum_{s=-\infty}^{+\infty} \frac{(-1)^s \hat{G}_s^{pq}(\xi)}{4} \left[\sum_{\gamma_1=\pm 1} \sum_{\gamma_2=\pm 1} J_{s+2\gamma_2}(c) J_{n\gamma_1+s}(a) I_{\frac{n\gamma_1-2\gamma_2}{2}}(b) \right] =$$

$$\frac{\hat{G}_0^{pq}(\xi)}{2} J_2(c) J_n(a) \left[I_{\frac{n-2}{2}}(b) + I_{\frac{n+2}{2}}(b) \right] + \frac{1}{2} \sum_{s=1}^{+\infty} \hat{G}_s^{pq}(\xi)$$

$$\left\{ I_{\frac{n-2}{2}}(b) \left[J_{n-s}(a) J_{2-s}(c) + J_{n+s}(a) J_{2+s}(c) \right] (-1)^s \right.$$

$$\left. + I_{\frac{n+2}{2}}(b) \left[J_{n-s}(a) J_{2+s}(c) + J_{n+s}(a) J_{2-s}(c) \right] \right\} \quad n \text{ even; } 0 \text{ otherwise,} \qquad (9$$

with $\hat{G}_{-s} = \hat{G}_s$ real. Unlike the LCA2 model, the SSA2 model requires the computation of a sum over s. For s=0, corresponding to the LCA2 model, Eq. (1) is found.

The SSA2 requires the computation of a sum because its second-order sub-kernel $\hat{\mathcal{N}}_2^{pq}(\xi, \phi_\xi)$ depends on the angle ϕ_ξ, whereas the LCA2 second-order sub-kernel is isotropic, since it is independent of $\phi - \phi_\xi$. This fundamental difference implies that the derivations led for the SSA2 model are more complicated than that of the LCA2 model. It is also important to note that Eq. (4) is valid for any kernel $\hat{\mathcal{N}}_2^{pq}(\xi, \phi_\xi)$ obeying the same properties as SSA2 or LCA2.

III. Numerical results

A. Numerical implementation

For incidence angles of interest for remote sensing applications, $\theta \in [0;60]°$, and for the VV and HH co-polarizations, this section presents numerical results of the incoherent BNRCS by assuming an anisotropic height spectrum given by the Elfouhaily et al. [14] model. Two radar frequencies are studied, f=5.3 GHz (C-band, sea relative permittivity ε_r=67+j35 [18]) and f=14 GHz (Ku-band, ε_r =47+j38 [18]).

The numerical evaluations of the BNRCSs $\{\sigma_{11,0}^{pq}(\theta;u), \sigma_{11,1}^{pq}(\theta;u), \sigma_{11,2}^{pq}(\theta;u)\}$ are rather simple. First, the isotropic $W_0(r)$ and anisotropic $W_2(r)$ parts of the correlation function are computed over $r \in [0;r_{max}]$. For frequencies f={5.3,14} GHz, the maximum radial distance $r_{max} \approx \{5,1\}$ meters. It decreases when the incidence angle decreases, the wind speed increases and the frequency increases. It is important to note that since the sea correlation function is independent of {θ,f}, $\{W_0(r), W_2(r)\}$ were computed and stored in a data file. In addition, the sampling over the radial distance r is done in a *logarithmic* scale with 200 samples.

The numerical evaluations of the BNRCSs $\{\sigma_{12,0}^{pq}, \sigma_{12,2}^{pq}\}$ are more complicated, because they require an additional integration over the sea wavenumber $\xi \in [\xi_{min}, \xi_{max}]$. We choose $\xi_{min}=0.25k_p$, which corresponds to the value for which the sea height isotropic spectrum falls down to 10^{-5} times its maximum, which occurs at k_p. The value ξ_{max} equals 4K. Thus, the double integration over $r \in [0;r_{max}]$ and over $\xi \in [\xi_{min}, \xi_{max}]$, is done in a *logarithmic* scale with 200x200 samples. Finally, the Fourier series coefficients defined by Eq. (2) are calculated by using a sampling step over $\phi - \nu\phi_\xi$ of 3 degrees. The BNRCSs require the computation of a sum over s from 0 to s_{max}. With the LCA model, s_{max}=0 whereas for the SSA model, s_{max} must be determined. This aspect is presented in details in [13]. It is shown that the integer s_{max} increases slightly with the angle θ, is few sensitive to the polarization and the order n of the harmonic. Typically, for $\theta \leq 30°$, $s_{max} \leq 3$ whereas for $\theta \in]30;60]°$, s_{max} reaches the maximum value 7 in average. Thus, the sum over s converges rapidly.

With these parameters, for a given incidence angle θ, on a PC with 4GB of RAM and a processor of 3 GHz, the computing time is of the order of 0.9 second. The scope of the paper is not to compare the different backscattering models with measurements. This was thoroughly already done in previous works [9, 12, 20].

B. Comparison of SSA2, LCA2 and SPM1

Figures 2 and 3 plot the harmonics of the BNRCS versus the incidence angle θ for f={14, 5.3} GHz, u_{10}=10 m/s and for VV and HH polarizations. The labels in the legend mean

- SSA11 corresponds to $\sigma_{11,n}^{pq}$ computed from the SSA-1 model with n={0,2} and pq={VV,HH},
- SSA11+12 corresponds to $\sigma_{11,n}^{pq} + \sigma_{12,n}^{pq}$ computed from the SSA2 model with n={0,2} and pq={VV,HH},
- LCA11 corresponds to $\sigma_{11,n}^{pq}$ computed from the LCA-1 model with $ n={0,2} and pq={VV,HH},
- LCA11+12+PPT corresponds to $\sigma_{11,n}^{pq} + \sigma_{12,n}^{pq}$ computed from the LCA2 model combined with the PPT with n={0,2} and pq={VV,HH},
- SPM-1 corresponds to $\sigma_{11,n}^{pq}$ computed with SPM and given by

$$\begin{cases} \sigma_{11,0}^{pq}(\theta;u) = 2 \left| \mathcal{N}_1^{pq}(\theta) \right|^2 \hat{W}_0(k_B)/k_B \\ \sigma_{11,2}^{pq}(\theta;u) = \sigma_{11,0}^{pq}(\theta;u) \hat{\Delta}(k_B) \end{cases}$$

As expected, the BNRCS decreases more quickly for HH polarization.

For near-nadir incidence angles, figures 2 and 3 reveal that the LCA11 and the SSA11 models are similar, which means that SSA11 reproduces the KA (Kirchhoff Approximation) reduced to the SPA (stationary Phase Approximation).

Theoretically, SSA11 does not reproduce the KA, but since the sea surface is highly conducting and the backscattering angle vanishes, the SPM polarization matrix is close to the Kirchhoff one.

It can be noted that by construction, the LCA11 model is the same as the KA+SPA model. For incidence angles ranging from 0 to approximately 20 degrees, only the gravity waves contribute to the scattering and therefore the KA+SPA can be applied. However, a smooth transition for scattering angles $\theta \in [20;40]°$ is observed, for which the KA+SPA model becomes invalid and the Bragg scattering regime (given by SPM) contributed increasingly. In this region, SSA11 tends to SPM, and the higher orders of SSA2 and LCA2 contribute. For the LCA2 model, this contribution is positive for the VV polarization, whereas it is negative for the HH polarization. For the SSA2 model, this contribution is negative for the VV polarization and it is weak, whereas it is positive for the HH polarization and it is much smaller than that of the LCA model. Thus, the behavior of the kernel of each model is very different.

It is important to note that the LCA2 results plotted in figures 2 and 3 use the PPT, which consists in adding the term $|\hat{\mathcal{N}}_2^{pq}|^2$ in Eq. (3). If the PPT is not applied, then for larger scattering angles, simulations not reported in this paper, show a non-physical behavior of the BNRCS for the HH polarization. With the SSA model, the results obtained with the PPT are the same as the ones plotted in figures 1 and 2. For a one-dimensional sea surface, as explained in details in the paper of Bourlier et al. [19], although the LCA kernel reaches the SPM and the KA+SPA limits and is tilt invariant, the BNRCS does not converge toward the Bragg regime. A theoretical explanation in given in the conclusion of [19]. Thus, the use of the PPT in the LCA model allows us to remove this drawback. This is why, in the paper of Mouche et al. [20], the LCA model with the PPT gives satisfactory results on the BNRCS.

C. Optimization of the SSA2 and LCA2 computation

Eqs. (1) and (4) require the computation of two-fold numerical integrations over the radial distance r and the sea wavenumber ξ. First, integrating over r, the resulting integrand depends then only on ξ. Plotting this integrand versus ξ, we observe that two wavenumbers $\{\xi_l, \xi_h\}$ mainly contribute to the scattering process. The first one is defined as $\xi_l=1.66k_p$ (low frequency), in which k_p corresponds to the wavenumber for which the sea *height* isotropic spectrum is maximum. In fact, $1.66k_p$ corresponds to the maximum of the *slope* isotropic spectrum (heigh spectrum multiplied by ξ^2). The second one is defined as $\xi_h=k_B$ (high frequency). Thus, the second-order BNRCS results from the inteference of two waves of wavenumbers $\{\xi_l, \xi_h\}$. More precisely, for $\xi=\xi_h$, one can observe that the adjacent wavenumbers also contribute to the scattering process, and we show that $\xi_h \Rightarrow \xi_h \in [k_B-\Delta_\xi;k_B+\Delta_\xi]$ with $\Delta_\xi=0.5k_B$. It is equivalent to multiply the sea spectrum by a pulse function centered around k_B and of width $2\Delta_\xi$.

Figure 4 plots the ratio $|\sigma_{12,n}^{pq}|/\sigma_{11,n}^{\tilde{pq}}$ of the SSA2 model versus the incidence angle θ, with different choices of the integration over ξ. The labels in the legend mean that

- for MP1, $\xi=\xi_l=1.66k_p$ for the integration,
- for MP2, $\xi=\xi_h$ for the integration with a sampling step of $0.1\ k_B$ ($n_\xi=11$),
- for MP3, $\xi=\{\xi_l, \xi_h\}$ for the integration,
- else $\xi \in [0.25\ k_p;4K]$ (full spectrum) with $n_\xi=200$ (number of samples).

As one can see, for low incidence angles, only the sea wavenumber $\xi=\xi_l$ contributes to the scattering process, whereas for moderate incidence angles (Bragg regime), both the low- (ξ_l) and high- frequencies (ξ_h) contribute. Moreover, the results are very close to that obtained from the full spectrum. Thus, with this new integration, the computing time is reduced to 0.07 second instead of 0.90 second, when the full spectrum is used.

Same simulations done with the LCA2 model and not reported here led to different conlusions. Indeed, the results computed from the LCA2+MP2 model are the same as the ones obtained from the LCA2 (full spectrum) model. This shows that only the high-frequency components of the sea spectrum contribute to the scattering process, unlike the SSA2 model, for which both the low- and high- frequency components contribute.

IV. CONCLUSION

In this paper, closed-form expressions of the Fourier coefficients of the BNRCS were expressed for a Gaussian process. Then, the "11" order, resulting from the correlation of the first-order scattered field, requires two independent numerical integrations over the wavenumber ξ (for the calculation of the height correlation function), and over the radial distance r. The "12" order, resulting from the cross-correlation between the first- and second- order scattered fields, requires two-fold numerical integrations over the radial distance r and over the wavenumber ξ, and one numerical angular integration for the computation of the Fourier series coefficients of the second-order kernel. The SSA2 and LCA2 kernels were tested for microwaves frequencies and different wind speeds. The numerical results showed that the SSA2 and LCA2 have different behaviors, and the correction from the "12" order is larger for the LCA2 model than for the SSA2 model. In addition, an optimization for the numerical integration over ξ was proposed, leading to a computing time of the "12" order less than 0.1 second on a standard office computer for a given wind speed, a given frequency and a given incidence angle.

REFERENCES

[1] B. F. Kur'yanov, "The scattering of sound at a rough surface with two types of irregularity," Sov. Phys. Acoust., vol. 8, pp. 252-257, 1963.

[2] W. Wright, "A new model for sea clutter," IEEE Trans. Ant. Prop., vol. 16, no. 2, pp. 217-223, 1968.

[3] G. Soriano and C.-A. Guérin, "A cutoff invariant two-scale model in electromagnetic scattering from sea surfaces," IEEE Trans. Geos. Rem. Sensing Letters, vol. 5, no. 2, pp. 199-203, 2008.

[4] N. Sajjad, A. Kenchaf, A. Coathanay and A. Awada, 2008, "An improved two-scale model for the ocean surface bistatic scattering,"

Paper presented at the International Geoscience and Remote Sensing Symposium, in USA, Boston, MA.

[5] S. Boukabara, L. Eymard, C. Guillou, D. Lemaire, P. Sobieski, and A. Guissard, "Development of a modified two-scale electromagnetic model simulating both active and passive microwave measurements: Comparison to data remotely sensed over the ocean", Radio Science, vol. 37, pp. 1063, 2002.

[6] T. M. Elfouhaily and C.-A. Guérin, "A critical survey of approximate scattering wave theories from random rough surfaces," Waves Random Complex Media, vol. 14, no. 4, pp. R1-R40, 2006.

[7] A. G. Voronovich, "Small slope approximation for electromagnetic wave scattering at a rough interface of two dielectric half-spaces," Waves in Random Media, vol. 4, no. 3, pp. 337-367, 1994.

[8] A. G. Voronovich, Wave scattering from rough surfaces. Germany: Springer series on Wave Phenomena (Second edition), 1999.

[9] A. G. Voronovich, "The effect of the modulation of Bragg scattering in small-slope approximation," Waves in Random Media, vol. 12, pp. 341-349, 2002.

[10] T. M. Elfouhaily, S. Guignard, R. Awadallah and D. R. Thompson, "Local and non-local curvature approximation: a new asymptotic theory for wave scattering," Waves Random Complex Media, vol. 13, no. 4, pp. 321-337, 2003.

[11] T. M. Elfouhaily and J. T. Johnson, "Extension of the local curvature approximation to third order and full tilt invariance," Waves Random Complex Media, vol. 16, no. 2, pp. 97-119, 2006.

[12] C. Bourlier, "Azimuthal harmonic coefficients of the microwave backscattering from a non-Gaussian ocean surface with the first-order SSA model," IEEE Trans. Geos. Rem. Sensing, vol. 42, no. 11, pp. 2600-2611, 2004.

[13] C. Bourlier and N. Pinel, "Numerical implementation of local unified models for backscattering from random rough sea surfaces," Waves in Random and Complex Media, vol. 19, no. 3, pp. 455-479, 2009.

[14] T. Elfouhaily, B. Chapron, K. Katsaros and D. Vandemark, "A unified directional spectrum for long and short wind-driven waves", J. Geo. Res., vol. 102, no. C7, pp. 781-796, 1997.

[15] F. J. Wentz, S. Peteherich and L. A. Thomas, "A model function for ocean radar cross section at 14.6 GHz," J. Geo. Res., vol. 89, pp. 3689-3704, 1984.

[16] A. Bentamy, P. Queffeulou, Y. Quilfen and K. Katsaros, "Ocean surface wind fields estimated from satellite active and passive microwave instruments", IEEE Trans. Geos. Rem. Sens., vol. 37, pp. 2469-86, 1999.

[17] A. A. Mouche, D. Hauser, J.-F. Daloze and C. Guerin, "Dual-polarization measurements at C band over the ocean: Results from airborne radar observations and comparison with ENVISAT ASAR data," IEEE Trans. Geos. Rem. Sens., vol. 43, no. 4, pp. 753-769, 2005.

[18] W. Ellison, A. Balana, G. Delbos, K. Lamkaouchi, L. Eymard, C. Guillou, and C. Prigent, "New permittivity measurements of seawater," Radio Science, vol. 33, pp. 639–648, 1998.

[19] C. Bourlier, N. Déchamps and G. Berginc, "Comparison of asymptotic backscattering models (SSA, WCA, and LCA) from one-dimensional gaussian ocean-like surfaces," IEEE Trans. Ant. Prop., vol. 53; no. 5, pp. 1640-1652, 2005.

[20] A. A. Mouche;, B. Chapron and N. Reul, "A simplified asymptotic theory for ocean surface electromagnetic wave scattering," Waves Random Complex Media, vol. 17, pp. 321-341, 2007.

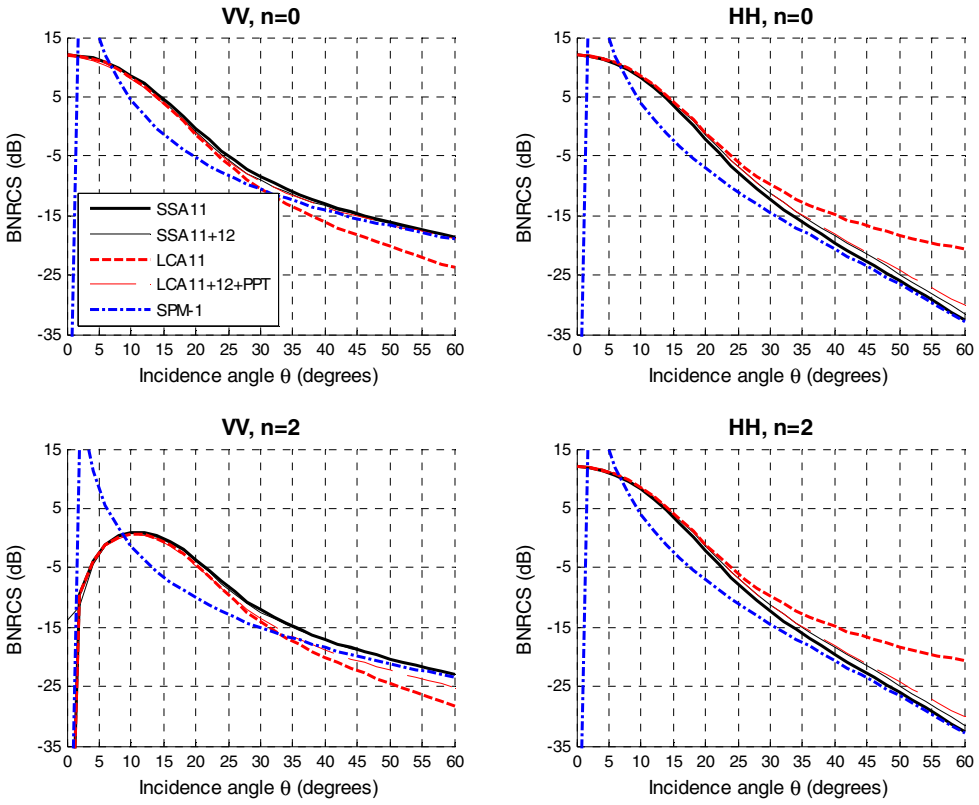

Figure 2. Harmonics of the BNRCS versus the incidence angle θ for f=14 GHz, u_{10}=10 m/s, VV (left) and HH (right) polarizations and for n={0 (top), 2 (bottom)}.

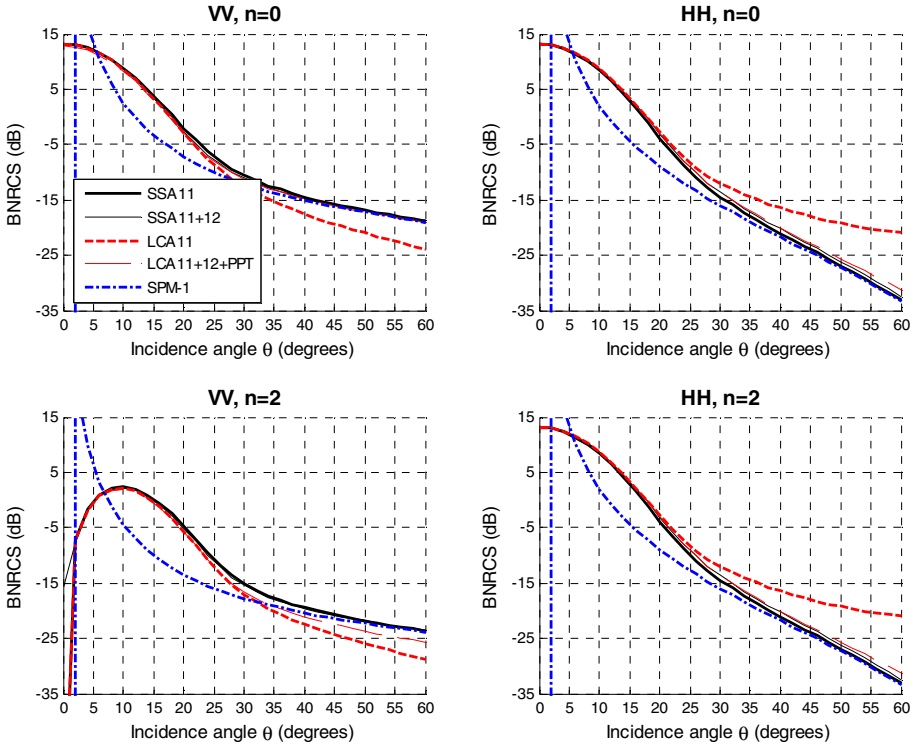

Figure 3. Same as in Figure 2 but for f=5.3 GHz.

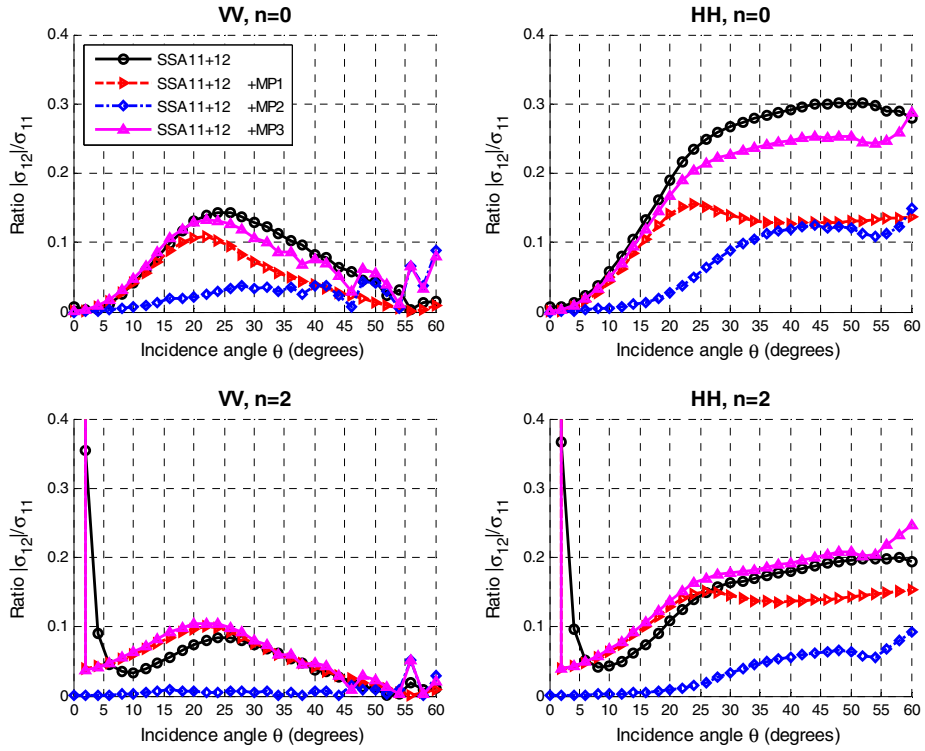

Figure 4. Ratio $|\sigma_{12,n}^{pq}|/\sigma_{11,n}^{\tilde{pq}}$ of the SSA2 model versus the incidence angle θ, with different choices of the integration over ξ.